Face morphing detection in the presence of printing/scanning and heterogeneous image sources¹

Matteo Ferrara, Annalisa Franco and Davide Maltoni

Department of Computer Science and Engineering, University of Bologna
via dell'Università, 50 – Cesena - Italy

Abstract

Face morphing represents nowadays a big security threat in the context of electronic identity documents as well as an interesting challenge for researchers in the field of face recognition. Despite of the good performance obtained by state-of-the-art approaches on digital images, no satisfactory solutions have been identified so far to deal with cross-database testing and printed-scanned images (typically used in many countries for document issuing). In this work, novel approaches are proposed to train Deep Neural Networks for morphing detection: in particular generation of simulated printed-scanned images together with other data augmentation strategies and pre-training on large face recognition datasets, allowed to reach state-of-the-art accuracy on challenging datasets from heterogeneous image sources.

1. Introduction

The widespread adoption of biometric identification techniques in the context of identity documents poses some concerns for the possibility of fraudulent misuses. Recent studies [1] [2] [3] [4] revealed that ePassports are particularly sensitive to the so called morphing attack, where the face photo printed on paper and provided by the citizen can be altered. Such attack was first described in [2] in the context of face verification at Automated Border Control (ABC) gates where two subjects cooperate to produce a morphed face image (mixing their identities) in order to obtain a regular travel document that could be exploited by both subjects (see Figure 1). Of course, in order to succeed in the attack, the morphed face image must be very similar to one of the two subjects (the one applying for the document) to fool the officer during the issuing process, but at the same time must contain enough features of the hidden subject to enable positive verification at the gate for both individuals.

The feasibility of this attack has been analyzed and confirmed by several researchers and some police agencies, thus making the development of proper countermeasures quite urgent.

One of the main challenges for the development of effective solutions for morphing detection is that typically the id photo, natively digital, is printed by the photographer and then scanned by the officer to be stored into the document chip. This Printing/Scanning process (P&S) alters the image information, removing most of the fine details (i.e. digital processing artifacts) that could help to detect morphing. Some preliminary studies, more widely discussed in the next section, show that morphing detection from digital images can be addressed to some extent, but P&S images are still difficult to manage [5]. Promising solutions have been recently obtained by using Deep Neural Networks (DNN), which proved to effectively detect and recognize faces in uncontrolled scenarios [6]. However, to reach a good

¹ The paper is currently under consideration at Pattern Recognition.

accuracy, DNN typically require a large training dataset. Unfortunately, in the context of morphing detection, it is difficult to collect large databases of samples: manually producing high quality morphed images is in general a boring and time-consuming activity. Moreover, due to the need of detecting morphing from P&S images, the costs/efforts for printing the images and scanning them again must be also considered. For this reason, most of the approaches in the literature exploit pre-trained deep networks as feature extractors, and build on the top of them traditional classifiers (e.g., SVM) that can be trained with relatively small datasets. The aim of this study is to investigate the possibility of artificially generating large sets of morphed images to train DNNs. In particular, this work focuses on the simulation of the P&S process which, coupled with the automatic generation of morphs, can produce large datasets for i) training new networks from scratch or ii) fine-tuning pre-trained DNNs such as AlexNet [7] or VGG [8]. Moreover, an extensive analysis of the network behavior with respect to genuine/morphed and digital/printed-scanned images enables a deeper understanding of the most relevant image features exploited for classification.

The rest of the paper is organized as follows: Section 2 discusses the state of the art; in Section 3 the procedure for automatic printed/scanned image generation is described. The DNNs used for the experiments are briefly introduced in Section 5 and the experimental results are reported and commented in Section 6. Finally, Section 7 draws some conclusions and discusses possible future research directions.

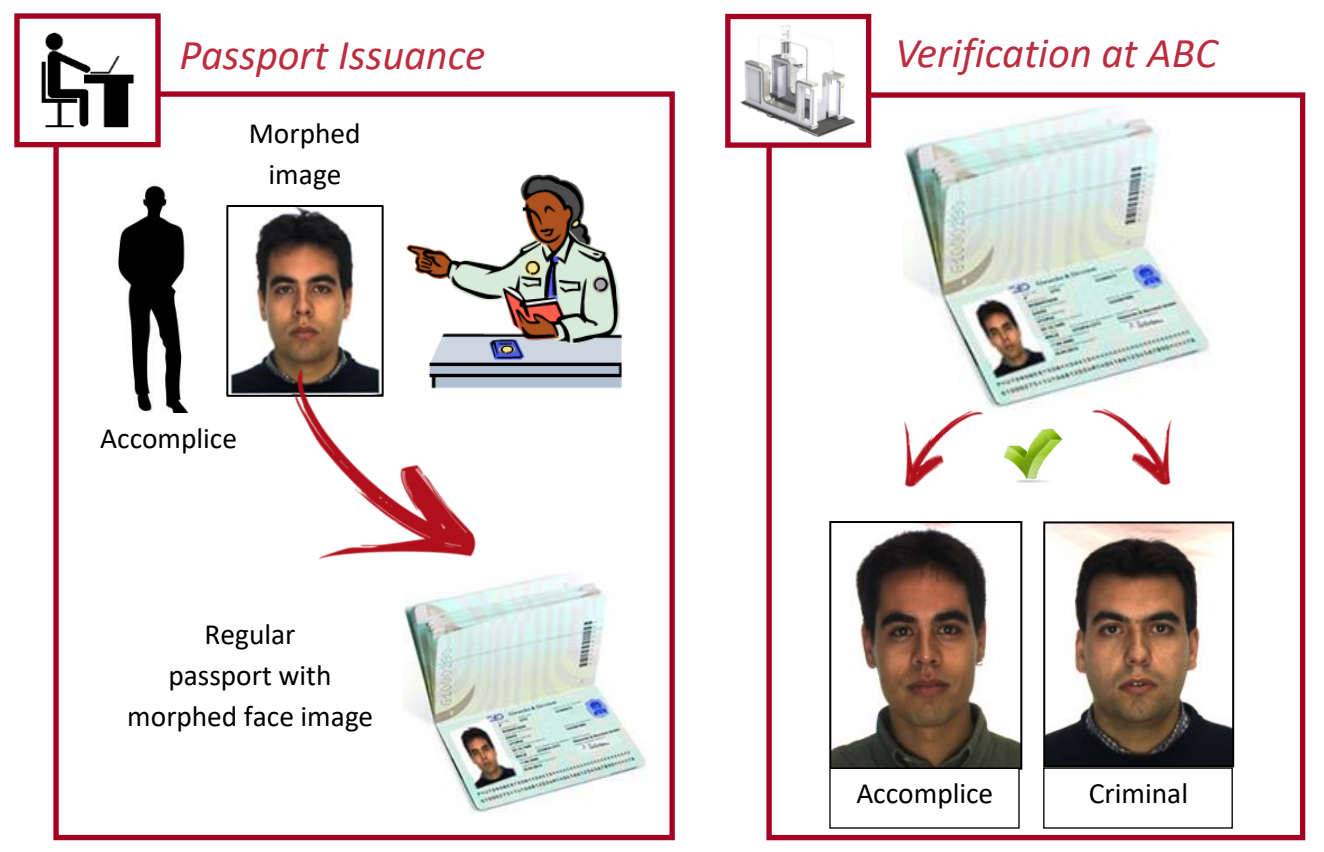


Figure 1: Morphing attack: the face image provided to the officer is visually very similar to the applicant (i.e. the accomplice), but also contains facial features of the criminal. Both subjects can use the document to transit through an ABC gate.

2. Related works and contribution

Although face morphing detection is a recently emerged research area, an increasing number of researchers are working on this topic and the related literature is constantly growing [9]. Existing techniques can be mainly framed in two categories:

- *single-image based*, where the presence of morphing alterations is detected on a single image, such as the id photo presented to the officer at enrolment time or the face image read from an e-document during verification at the gate;
- *image-pair based* (a.k.a. *differential morphing detection*), where the comparison between a live image (e.g., acquired at the gate) and that stored on the e-document is exploited for morphing detection.

Most of the literature approaches belong to the first category. The works based on handcrafted features mainly try to analyze the small image degradations produced by the morphing process. In [10] the authors propose a technique for morphing detection based on the analysis of micro-texture variations using Binarized Statistical Image Features (BSIF): an SVM classifier is trained to discriminate genuine/morphed faces. The authors of [11] argue that the morphed images are characterized by a different texture with respect to the unaltered ones and that a progressive JPG compression can further highlight this aspect; the image content is finally represented by different corner features exploited for classification. In [12] [13] [14] morphing detection is based on Benford features extracted from quantized DCT coefficients, in [15] key-points features (such as SURF, ORB, FAST, etc.) are used, while in [16] and [17] LBP features are analyzed. An interesting outcome of [16] is that low-level features are not robust when used in cross-database testing or in the presence of simple image manipulations (e.g., rescaling). The authors of [18] and [19] exploit the principle of image source identification for morphing detection, observing that a morphing is a computer-generated image and its sensor-pattern noise is different from that of a real image. Other works make use of topological analysis of facial landmarks to detect alterations introduced by morphing [20] [21]; the idea is interesting in principle, but overall the results obtained are unsatisfactory for real application. Most of the referred approaches, when tested on digital images only, provide good classification performance, but the use of different databases and different evaluation metrics make a comparison quite difficult.

Deep learning techniques based on Convolutional Neural Network (CNN) have been proposed for face morphing detection [17] [22] [23] [24]. The authors of [17] evaluate some networks, pre-trained for face recognition, as feature extractor for digital images, without performing any fine-tuning on the specific morphing detection task, while in [22] two pre-trained networks, AlexNet [7] and VGG19 [8], are used for feature extraction after a fine-tuning step. The authors perform tests on both digital and P&S images and the experimental results clearly confirm that the second type of images represent the main challenge for morphing detection. In [23] some CNNs are used for morphing detection from digital images; the accuracy of pre-trained networks is compared to that of networks learned from scratch, finally leading to the conclusion that pre-trained networks are more robust for this task. The authors of [24] analyze the accuracy of pre-trained networks against semantic (partial morphing on some specific face regions) and black box attacks (partial occlusions), and highlight, for the two kind of images, the most relevant regions analyzed by the networks for classification. Finally the authors of [25] combine features of different nature, hand-crafted and extracted by CNNs, demonstrating that a substantial improvement in detection performance can be achieved by their integration.

To the best of our knowledge, only two approaches perform morphing detection by image-pair comparison. The first approach has been introduced in [26] [27] where the inverse process of morphing (called demorphing) is adopted to revert the effects produced by morphing. The demorphing technique proved to be effective both on digital and P&S images. The same detection scheme has been considered in [28] where different features are evaluated both for single-image and differential morphing detection.

Overall, an analysis of the literature allows to identify two major challenges for morphing detection techniques: i) robustness to the P&S process; ii) ability to generalize across different databases [29]. The present work mainly focuses on these two aspects. In particular, this paper provides the following contributions:

- Adoption of the P&S simulation model proposed in [30] for data augmentation (to the best of our knowledge this is the first attempt of P&S simulation in this context), enabling the possibility of producing training images without the cost/effort of the real P&S process. Such simulation produces a significant performance improvement on morphing detection from P&S images.
- Extensive experiments using four different well-known DNN architectures on three real test datasets. In this work, we perform an extensive analysis of CNNs pre-trained on large scale face recognition datasets, proving their superiority when dealing with P&S images.
- Comparison between direct classification after network fine-tuning and use of the network for feature extraction only, coupled with an external classifier.
- Even if a direct comparison is not feasible, because of the lack of P&S public databases, the performance of the proposed solution on P&S images compares favorably with other state-of-the-art approaches (Table 7).

3. Automatic image generation

In order to exploit the great potential of CNNs for classification, a very large set of images is typically needed and usually data augmentation techniques are applied [31] to increase the number of samples available for training; geometric and photometric transformations are the most frequently adopted modifications. In the context of morphing detection, the network training requires both real and morphed image samples, possibly in the two formats (digital and P&S). To avoid the effort/cost of collecting a large dataset we proposed novel techniques for automatically generating high quality morphed face images (Section 3.1) and simulating the P&S process (Section 3.2).

3.1. Face morphing

Morphed images can be obtained quite easily using one of the many existing tools and plugins (e.g., Sqirlz Morph [32]). However, the systematic generation of morphed images with specific characteristics can be better realized by ad hoc techniques. Here we adopt the approach described in [26] which includes an automatic image retouching phase to minimize visible artifacts. Given two images I_0 and I_1 , the process generates a set of frames $\mathbb{M} = \{I_\alpha, \alpha \in \mathbb{R}, 0 < \alpha < 1\}$ representing the transformation of the first image (I_0) into the second one (I_1) (see Figure 2). In general, each frame is a weighted linear combination of I_0 and I_1 , obtained by geometric warping of the two images based on corresponding landmarks and pixel-by-pixel blending. Formally:

$$I_{\alpha}(\mathbf{p}) = (1 - \alpha) \cdot I_0 \left(w_{P_{\alpha} \to P_0}(\mathbf{p}) \right) + \alpha \cdot I_1 \left(w_{P_{\alpha} \to P_1}(\mathbf{p}) \right), \tag{1}$$

where:

- **p** is a generic pixel position;
- α is the frame weight factor (representing the presence of the two contributing subjects);
- P_0 and P_1 are the two sets of landmarks in I_0 and I_1 , respectively;
- P_{α} is the set of landmarks aligned according to the frame weight factor α ;
- $w_{B\to A}(\mathbf{p})$ is a warping function.

A number of different morphed images can be obtained according to the value of the weighting factor α (i.e. the weight of the two subjects in the combination) as shown in Figure 2.

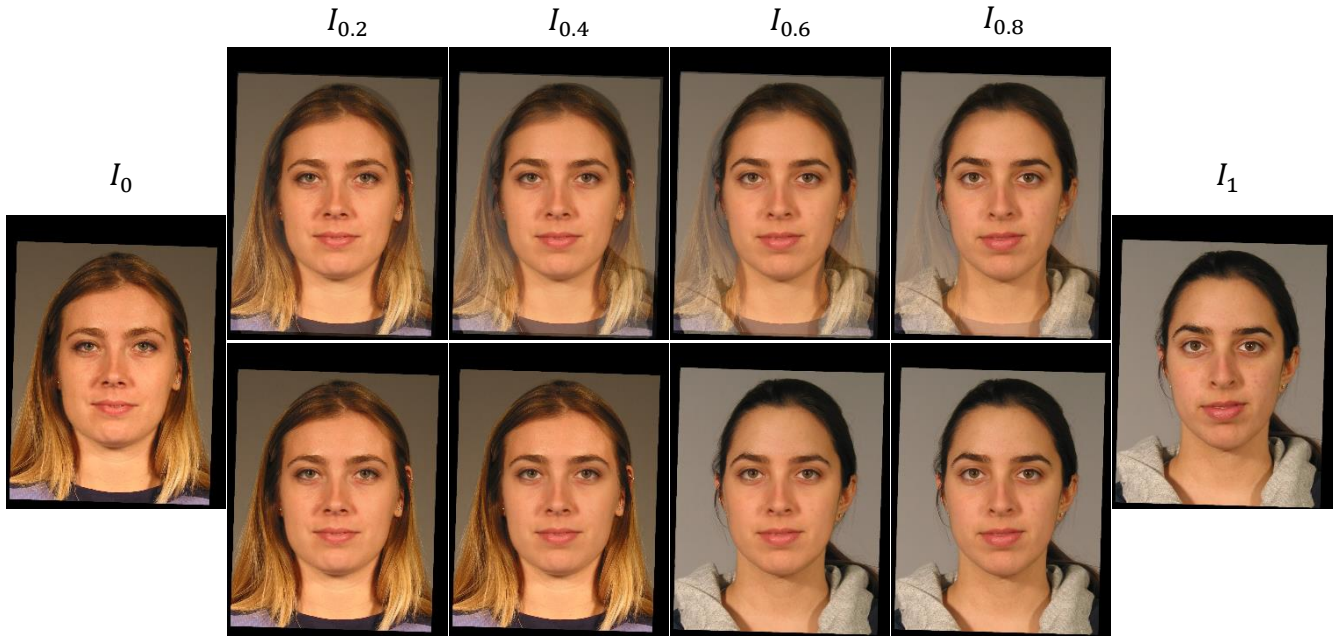


Figure 2: Example of morphed frames obtained by the morphing procedure, gradually moving from I_0 to I_1 (first row). In the second row the result of the automatic retouching process used to remove visible artifacts is shown.

3.2. Modeling the printing and scanning process

The P&S process is quite complex: i) digital images are first conveyed to the physical, continuous domain and then ii) re-digitalized and discretized by the scanning process. The image alterations introduced involve both pixel value distortions (i.e. luminance, contrast and gamma corrections, chrominance variations and blurring of adjacent pixels) as well as minor geometric alterations due to the positioning on the scanner surface.

Focusing on the pixel value distortion, according to the model proposed in [30] the P&S process of a generic digital image I produces a modified, discrete version of the image \tilde{I} as:

$$\tilde{I}(\mathbf{p}) = K[I(\mathbf{p}) * \tau_1(\mathbf{p}) + (x(\mathbf{p}) * \tau_2(\mathbf{p})) \cdot N_1] \cdot s(\mathbf{p}), \tag{2}$$

where:

- Function *K* represents the responsivity of the acquisition device;
- $s(\mathbf{p})$ is the sampling function which characterizes the digitalization process of the continuous printed image;
- τ_1 models the system point spread function $\tau_1(\mathbf{p}) = \tau_P(\mathbf{p}) * \tau_S(\mathbf{p})$ where $\tau_P(\mathbf{p})$ and $\tau_S(\mathbf{p})$ represent the point spread function of printer and scanner, respectively;
- τ_2 is a high-pass filter used to represent higher noise variance near the edges;
- N_1 is a white Gaussian random noise.

The following responsivity function *K* is adopted:

$$K(x) = \omega \cdot (x - \beta_x)^{\gamma} + \beta_K + N_2(x)$$
(3)

It includes color adjustments coefficients (β_x and β_K), gamma correction (γ) and a noise component $N_2(x)$ whose power is related to pixel intensity (usually higher noise on dark pixels is observed due to the different sensors' sensitivity to the image reflectivity).

Due to some device-dependent unknown parameters, the adaption of this model to real cases is not straightforward. In particular, the point spread functions of the devices (τ_P and τ_S in Eq. (2)) are not available, and they are approximated by two Gaussian blurring filters of size k_1 , k_2 and standard deviation σ_1 , σ_2 .

The model is quite flexible and allows to modify different image characteristics, related to both visual quality and low-level signal content. Figure 3-Figure 6 show the impact of the different model parameters on the result. In particular, ω mainly controls the image contrast and brightness (see Figure 3), while the overall system gamma, i.e. the combined effect of all gamma values applied to the imaged by the printing/scanning devices, can be adjusted by properly tuning γ (see Figure 4). Further variations to image color and saturation can be obtained though β_K and β_X parameters (see Figure 5). Finally the parameters of the Gaussian smoothing filter (k and σ) produce the most evident modification introduced by the P&S process, i.e. the blurring effect represented in Figure 6.





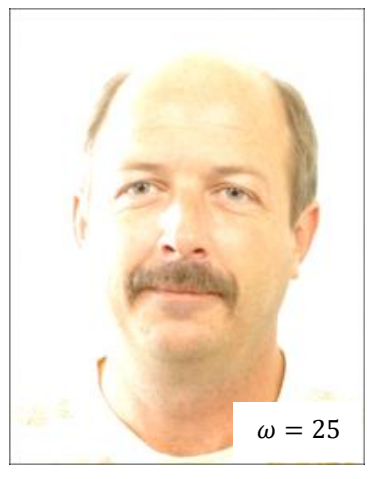


Figure 3: variation of ω parameter in the P&S simulation model applied to Figure 7.(a): this parameter mainly affects image contrast and brightness.

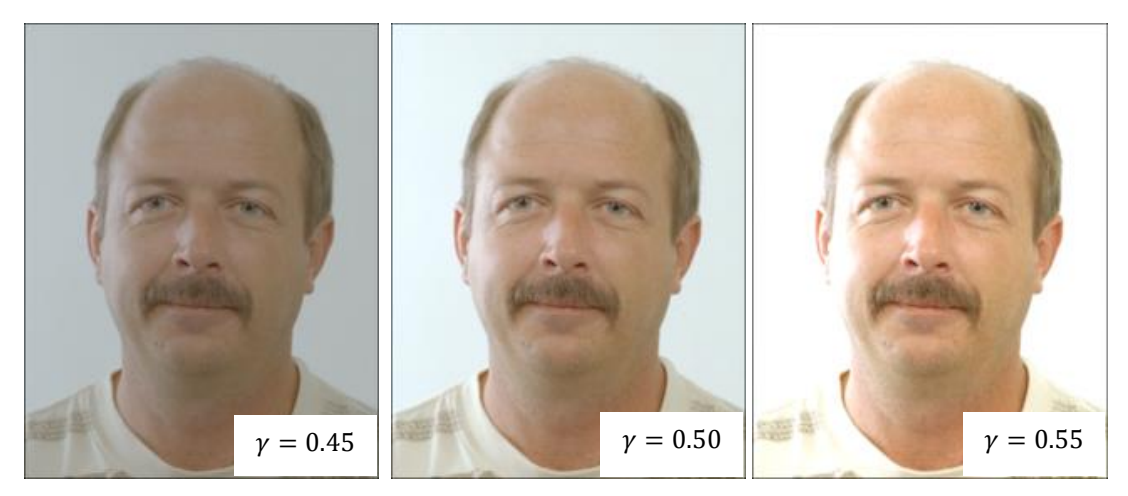


Figure 4: variation of γ in the P&S simulation model applied to Figure 7.(a): this parameter regulates the gamma corrections produced by the printing and scanning devices.

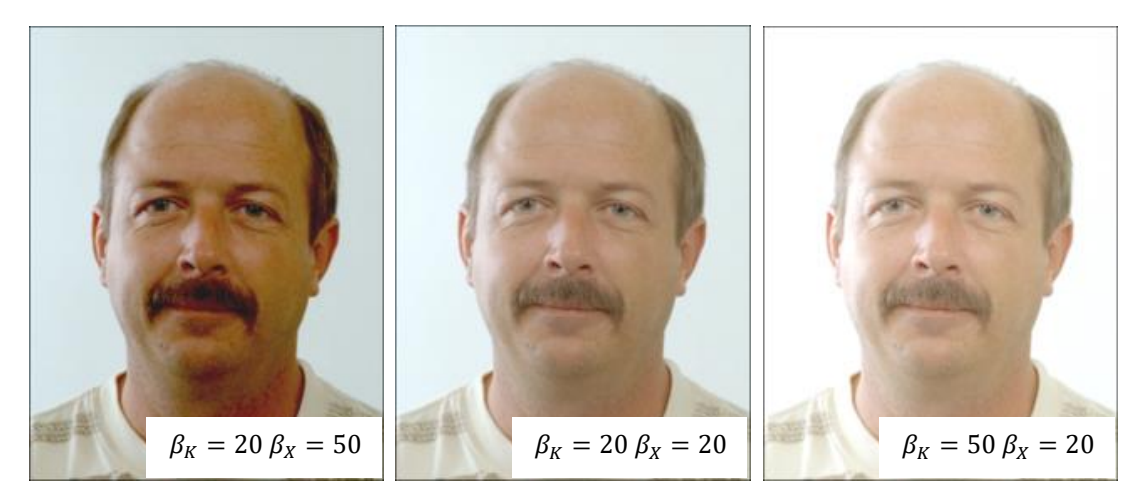


Figure 5: variation of β_K and β_X in the P&S simulation model applied to Figure 7.(a): these parameters control the image color and saturation.

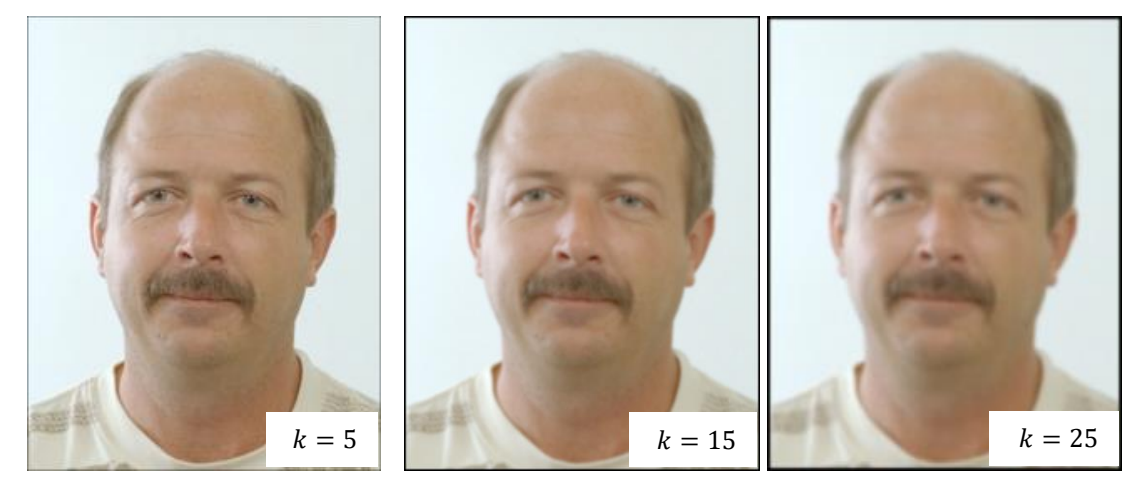


Figure 6: variation of k in the P&S simulation model applied to Figure 7.(a): this parameter controls the amount of image blurring.

In Figure 7 a real P&S image is compared with a simulated P&S image of the same digital image. The image spectrum is also reported to appreciate the low-level signal modifications produced by the P&S process. As clearly visible in the example, the digital image is much richer of fine details (high

frequencies) which are noticeably attenuated after P&S. The spectrum of the simulated P&S image (Figure 7.(f)) is quite similar to that of the real one (Figure 7.(e)). We can quantify the similarity between the image spectra adopting commonly used metrics such as the spectral angle [33] (a measure of distance between two spectra) or the correlation value. If we compare the digital image and the real P&S of Figure 7, the spectral angle is quite high (0.69) with a correlation value of 0.77. The similarity between the real P&S and the simulated one is much higher, as confirmed by the smaller spectral angle (0.38) and a higher correlation value (0.93).

The parameters used for image generation (see Table 1) have been chosen in order to produce images visually similar to the real P&S ones ($MorphDB_{P\&S}$ database described in Section 4.2), but no specific optimizations have been carried out (see Figure 7).

Table 1: Parameter values used in the P&S simulation process.

Parameter	Value
ω	15.5
eta_X	20
eta_K	20
γ	0.5
k_1, k_2	3
σ_1 , σ_2	1.2

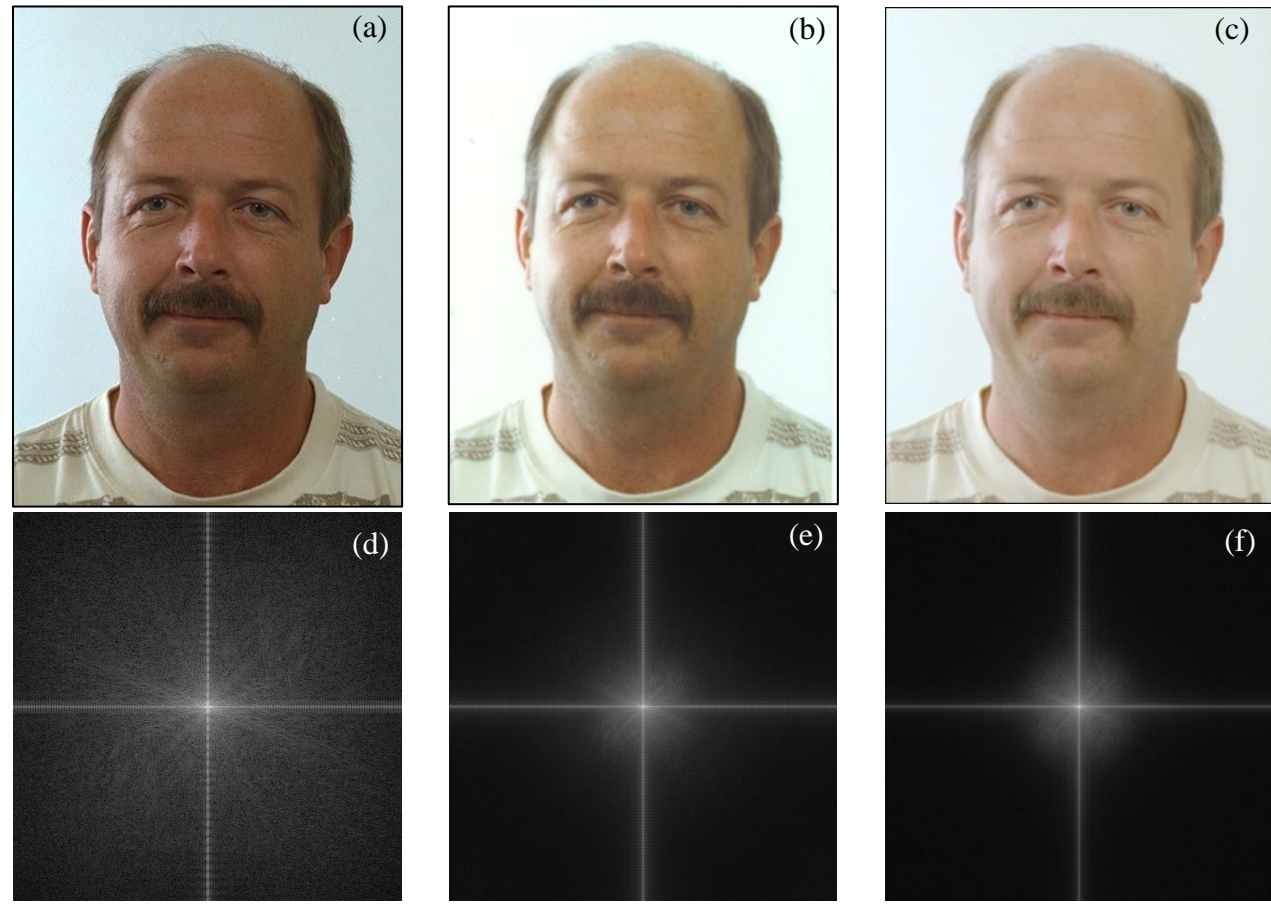


Figure 7: For the digital image (a) the result of the real (b) and simulated (c) P&S processes is provided. The corresponding image spectrum is also given for the digital image (d), the real (e) and the simulated P&S (f).

4. Databases

4.1. Training sets

For network training we used the Progressive Morphing Database (PMDB) described in [26]. It contains 6000 morphed images automatically generated starting from 280 different subjects selected from the AR [34], FRGC [35] and Color Feret [36] [37] databases using different morphing factors ($\alpha \in \{0.1, 0.15, 0.2, 0.25, 0.3, 0.35, 0.4, 0.45\}$ in Eq. (1)).

Since PMDB contains a different number of genuine and morphed images, a new balanced database (called *Digital*) has been derived as follows:

- 1. two images of each subject are chosen resulting in 560 genuine images;
- 2. 560 morphed images are randomly selected from the PMDB morphed images.

The P&S process has been simulated by applying the procedure described in Section 3.2 on all *Digital* images; we will refer to this dataset as $\widetilde{P\&S}$.

4.2. Test sets

The models trained on the datasets introduced in Section 4.1 are then tested on the following (separated) databases:

- *MorphDB_D* [26]: it consists of 130 genuine images (not morphed) and 100 morphed images (50 males and 50 females) produced with a significant manual intervention in order to minimize visible artifacts (see Figure 8).
- $MorphDB_{P\&S}$ [26]: P&S version of $MorphDB_D$. The images have been printed on high quality photographic paper by a professional photographer and then scanned (see Figure 9).
- *Biometix* [38]: a public dataset of 1082 morphed images obtained starting from 917 genuine images (of different subjects) chosen from the FERET database [36] [37] (see Figure 10).





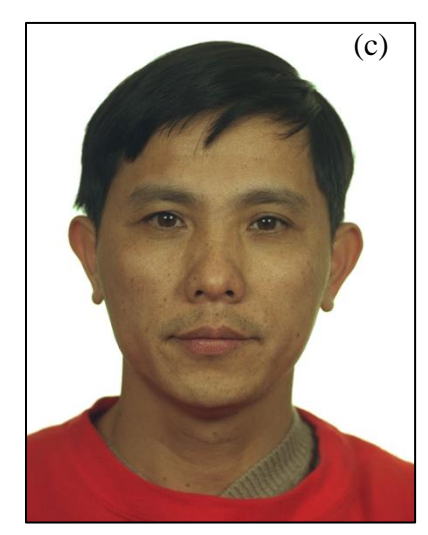


Figure 8: Images from $MorphDB_D$ database: digital version of genuine images of two subjects (a) and (c) and the resulting morphed image (b).







Figure 9: Images from *MorphDB_{P&S}* database: P&S version of the images reported in Figure 8.

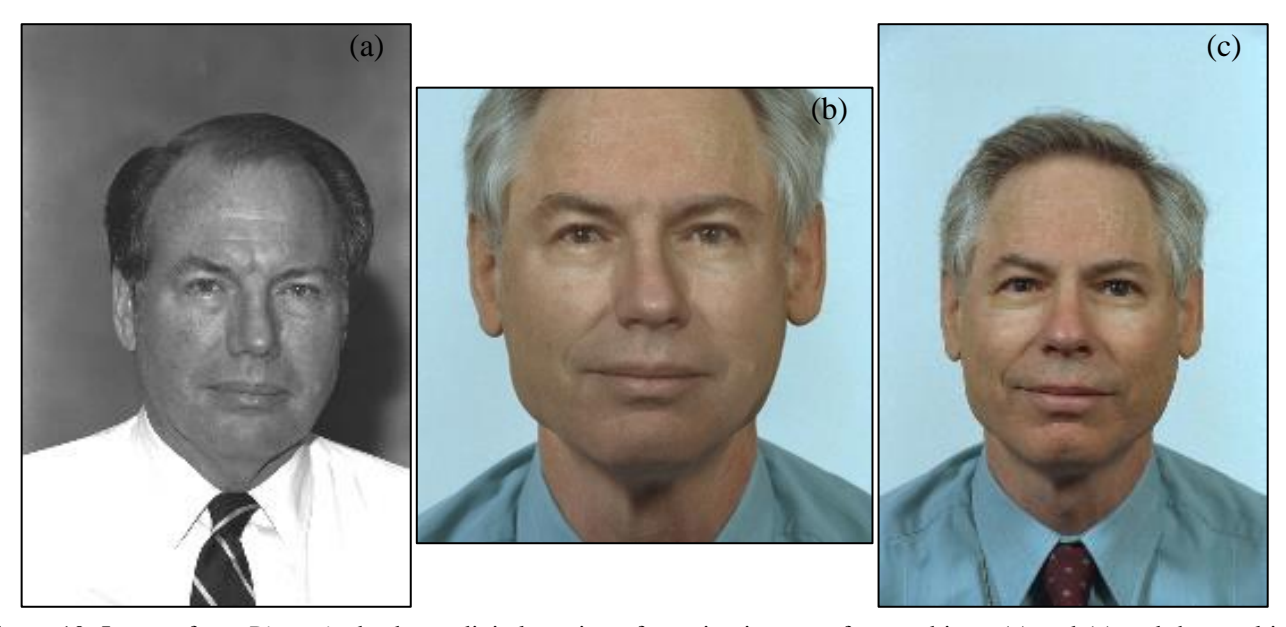


Figure 10: Images from *Biometix* database: digital version of genuine images of two subjects (a) and (c) and the resulting morphed image (b).

4.3. Data normalization

Since face images come from various sources presenting different size and resolution, it is important to normalize them before processing (see Figure 11). For this reason, each image is normalized as follows:

- 1. the eye centers and the nose tip are detected using Neurotechnology VeriLook SDK 10.0 [39];
- 2. the image is resized to obtain an eye center distance of 150 pixels;
- 3. a sub-image of size 350×400 pixels is cropped centered on the nose tip.

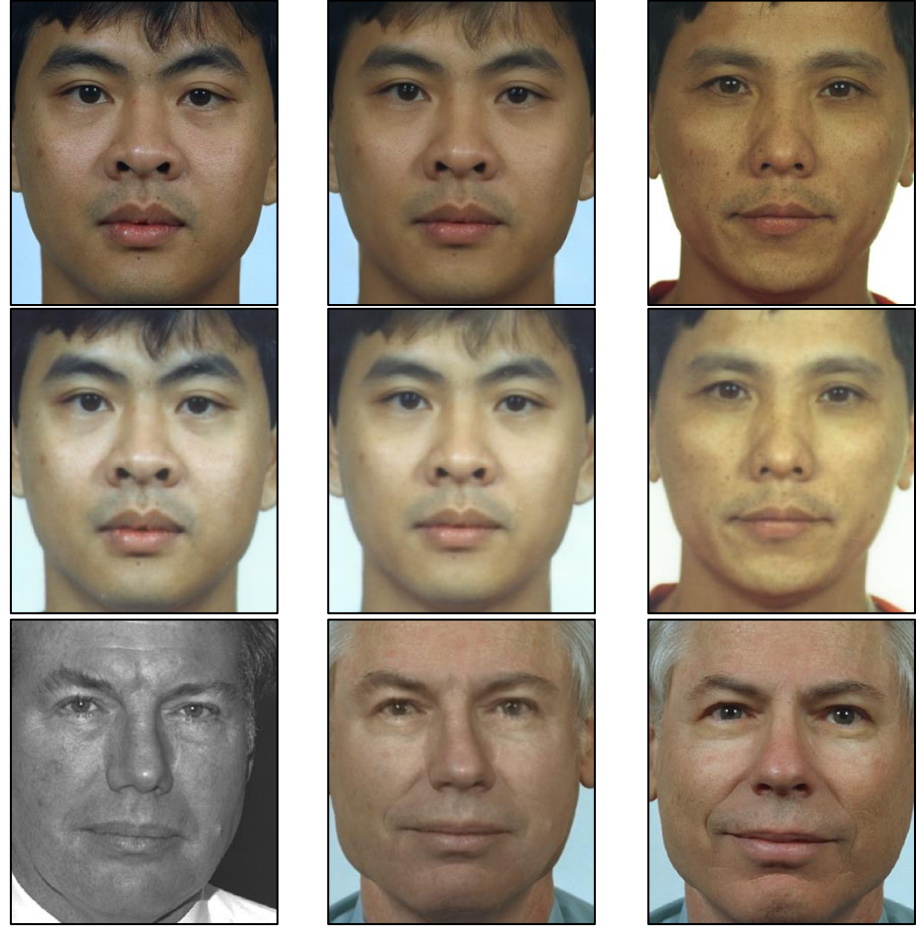


Figure 11: Normalized images from Figure 8 (first row), Figure 9 (second row) and Figure 10 (third row).

4.4. Data augmentation

Both training databases (Digital and P&S) contain 1120 images, not many for an effective network training. To increase the number of samples, data augmentation is applied obtaining different augmented databases (see Table 2). In particular, the following transformations are applied:

- horizontal mirroring;
- rotation centered on the nose tip $(\{-5^{\circ},0^{\circ},+5^{\circ}\})$;
- horizontal and vertical translation $(\{-1,0,+1\})$;
- multi-crop, i.e. extracting from each image (size 350×400) five sub-images corresponding to the four corners and the central region [7]. The crop size is fixed according to the image input size of the specific network (see Section 5). In the tests where multi-crop is not enabled, only the central region is used.

	P&S	Data Augmentation					# Images		
Name	Simulation	Horizontal Mirroring	Rotation	Horizontal and Vertical Translation	Multi-crop	Genuine	Morphed	Total	
Digital						560	560	1120	
P&S	\checkmark								
$Digital_{Au}$		$\sqrt{}$	√	V		30240	30240	60480	
$\widetilde{P\&S_{Au}}$	V	$\sqrt{}$	√	V					
$Digital_{Mc}$		\checkmark	V		$\sqrt{}$	16800	16800	33600	
$\widetilde{P\&S_{Mc}}$	$\sqrt{}$	$\sqrt{}$	V		$\sqrt{}$				

5. Deep Neural Networks for morphing detection

In this work we considered different well-known pre-trained deep neural networks (see Table 3). The first two networks, already used for morphing detection in previous works [22] [23], have been trained on natural images (i.e. ImageNet [40]) and therefore the learned filters are not specific for face representation. The last two networks are state-of-the-art models trained on very large face datasets: we can expect that the filters in the low and intermediate levels of these networks are capable of extracting very powerful face feature that can be exploited for morphing detection.

The last layer of all the considered architectures has been changed to deal with a two class problem (morphed vs genuine): as a consequence, the corresponding weights need to be learned from scratch.

Name	Architecture		Input		
T (MILLE	THE MICE VALUE	Image Type	Database name	Database size	image size
AlexNet [7] [41]	AlexNet - BVLC version	Natural	ImageNet [40], specific	1.2M	227 × 227
VGG19 [8]	VGG – 19 weight layers	- \	ILSVRC subsets [42]		224 × 224
VGG-Face16 [43]	VGG – 16 weight layers [8]	Face	VGG-Face dataset [43]	2.6M	224 × 224
VGG-Face2 [44]	ResNet-50 [45]		VGG-Face 2 dataset [44]	More than 3M	

Table 3: Neural networks used in the experimentation.

5.1. Fine-tuning

Starting from the pre-trained networks, a first fine-tuning step has been performed on $Digital_{Au}$ and $Digital_{Mc}$ datasets, separately, for 5 epochs each. Therefore, for each network architecture, we obtained two differently tuned networks able to detect digital morphed images but presenting poor results on P&S ones (see Section 6.2). To overcome this limit, a second fine-tuning step has been performed on $P \& S_{Au}$ and $P \& S_{Mc}$ datasets, for a single epoch each. For both fine-tuning stages, we used SGD optimization with a fixed learning rate of 0.0001 and a momentum of 0.9.

At test time, if multi-crop augmentation were used during training, the prediction probabilities are calculated as the average probabilities across five sub-images (i.e. the four corners and the central region) cropped from the normalized 350×400 image. Otherwise only the central region is used for classification.

5.2. Feature extraction with external classification

As an alternative to fine tuning, we also tested the above models as feature extractors coupled with external classifiers, As suggested in [22], the features from the first fully connected layer of all fine-tuned networks (see Section 5.1) are used with two conventional classifiers such as Linear SVM [46] and P-CRC [47] (both using default parameters). Since their training does not scale well with respect to the number of patterns, the features used to train the two classifiers are extracted from the training datasets without augmentation (i.e. *Digital* and $\widetilde{P\&S}$ in Section 4.1).

6. Experiments

Several experiments have been carried out to evaluate the robustness of DNNs for morphing detection with respect to: i) cross-database testing and ii) P&S images.

6.1. Testing protocol and performance indicators

For each experiment genuine and morphed face images are used to compute Bona Fide (BPCER) and Attack Presentation Classification Error Rates (APCER), as defined in [48].

The following performance indicators are calculated:

- Accuracy: the percentage of face images correctly classified as genuine or morphed;
- Equal-Error Rate (EER): the error rate for which both BPCER and APCER are identical;
- BPCER@APCER=p%: the lowest BPCER for APCER $\leq p\%$;
- Detection Error Tradeoff (DET) curve: the plot of APCER against BPCER.

6.2. Evaluating DNNs on classification

Table 4 reports the results obtained in terms of accuracy, EER, and BPCER (at different levels of APCER) as a function of i) the testing database, ii) the network and iii) the training set used. The corresponding DET curves are provided in Figure 12 and Figure 13.

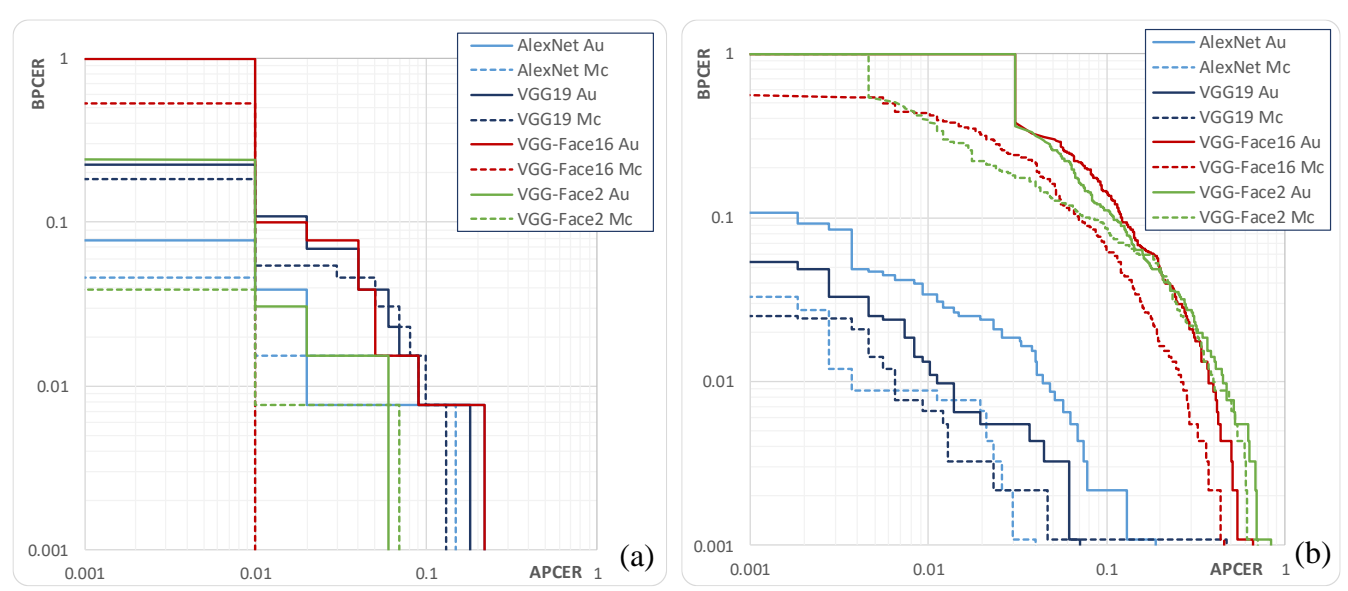


Figure 12: DET curves measured for the evaluated networks trained with digital images (Digital) using different data augmentation strategies (Au, Mc) on $MorphDB_D(a)$ and Biometix(b) databases.

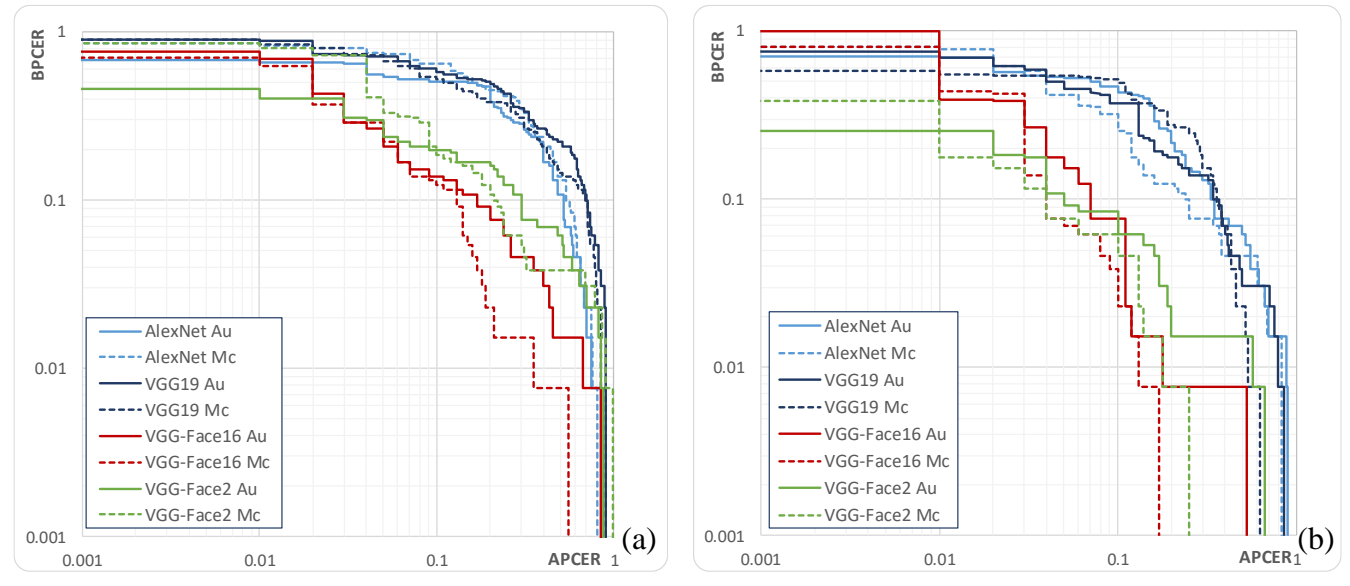


Figure 13: DET curves measured for the evaluated networks with different data augmentation strategies (Au, Mc) on $MorphDB_{P\&S}$: (a) results with the Digital training set, (b) results with the $Digital + \widetilde{P\&S}$ training set.

Table 4: Performance indicators of the evaluated networks on the testing databases using different training sets. The best result on each test database is highlighted in bold.

Test	Net	Training	Accuracy (%)	EER	BPCER (%) at			
1050				(%)	APCER=10%	APCER=5%	APCER=1%	
	AlexNet	$Digital_{Au}$	98.3	1.8	0.8	0.8	3.8	
		$Digital_{Mc}$	96.1	1.3	0.8	1.5	1.5	
	VGG19	$Digital_{Au}$	92.2	3.9	0.8	3.8	10.8	
$MorphDB_D$, 5519	$Digital_{Mc}$	94.3	4.3	0.8	3.1	5.4	
	VGG-Face16	$Digital_{Au}$	93.9	3.9	0.8	1.5	10.0	
	, 55 1 466 15	Digital _{Mc}	97.4	0.9	0.0	0.0	0.0	
	VGG-Face2	$Digital_{Au}$	95.2	1.8	0.0	1.5	3.1	
		Digital _{Mc}	93.0	0.9	0.0	0.8	0.8	
	AlexNet	$Digital_{Au}$	97.8	2.3	0.2	0.9	3.4	
		Digital _{Mc}	99.3	0.9	0.0	0.0	0.9	
	VGG19	$Digital_{Au}$	98.0	1.1	0.0	0.3	1.3	
Biometix	, 001)	$Digital_{Mc}$	98.9	0.8	0.1	0.1	0.7	
	VGG-Face16	$Digital_{Au}$	86.2	11.5	14.3	31.1	-	
		Digital _{Mc}	90.7	8.4	6.3	16.0	43.4	
	VGG-Face2	$Digital_{Au}$	89.2	10.5	11.1	25.9	-	
		Digital _{Mc}	90.7	9.4	8.5	13.0	39.7	
		$Digital_{Au}$	43.5	28.7	50.8	53.8	66.2	
	AlexNet	Digital _{Mc}	43.5	32.7	64.6	74.6	83.1	
		$Digital_{Au} + P \widetilde{\&S_{Au}}$	67.4	20.9	43.1	52.3	70.0	
		$Digital_{Mc} + P\widetilde{\&S_{Mc}}$	83.5	13.9	25.4	41.5	77.7	
		$Digital_{Au}$	47.0	32.7	57.7	71.5	89.2	
	VGG19	Digital _{Mc}	44.3	30.4	52.3	66.9	84.6	
		$Digital_{Au} + P \widetilde{\&S_{Au}}$	60.4	18.2	36.9	45.4	70.0	
$MorphDB_{P\&S}$		$Digital_{Mc} + P\widetilde{\&S_{Mc}}$	56.5	24.8	49.2	54.6	55.4	
in a spine a radio		$Digital_{Au}$	60.4	12.7	13.8	20.8	69.2	
	VGG-Face16	Digital _{Mc}	56.5	11.3	12.3	22.3	63.1	
		$Digital_{Au} + P \widetilde{\&S_{Au}}$	89.6	7.3	7.7	15.4	39.2	
		$Digital_{Mc} + P \widetilde{\&S_{Mc}}$	93.5	6.1	2.3	6.9	43.8	
		$Digital_{Au}$	51.7	16.5	20.0	23.8	40.0	
	VGG-Face2	Digital _{Mc}	45.7	15.7	18.5	33.1	80.0	
		$Digital_{Au} + \widetilde{P\&S_{Au}}$	74.3	8.2	6.2	9.2	25.4	
		$\widetilde{Digital_{Mc}} + \widetilde{P\&S_{Mc}}$	86.5	6.1	4.6	7.7	17.7	

The results show a variable behavior over different test databases. The performance measured over the two digital datasets $MorphDB_D$ and Biometix are good for all the evaluated networks, even if here the ImageNet pre-trained models (AlexNet and VGG-19) often achieve the best results. We argue that to detect artifacts and traces of digital manipulations that characterize digital morphed images, the general filters learned from natural images can be even more powerful than specific filters optimized for invariant face recognition. This observation is aligned with the outcomes of [23].

The discrepancy between $MorphDB_D$ and Biometix datasets is probably due to the different morphing techniques used in the two databases (see Figure 14). The $MorphDB_D$ contains high quality morphed images, where an accurate manual intervention removed most of the visible artifacts (see Figure 8); such a smooth result is also obtained by the automatic procedure designed to create the training images of the PMDB. On the other hand, Biometix database contains morphed images of a lower visual quality, with

artifacts (see Figure 10) which are not properly represented in the training set, and this is the probable cause of failure of some nets.



Figure 14: Examples of low quality morphed images from *Biometix* database with clearly visible artifacts.

The test on *MorphDB_{P&S}*, allows to evaluate the performance when the P&S process comes into play. In general, the results show that networks trained only on digital images are not able to deal with P&S images; all the architectures suffer from this issue and provide quite bad results. Exploiting simulated P&S images for network training allows in some cases to obtain a significant improvement (e.g., the accuracy of VGG-Face16 network trained with multi-crops grows from about 56% to 93%); these results are quite encouraging if we consider that no real P&S images have been used during training. Overall an accuracy of 85-90% can be reached with reasonable values of EER and BPCER at APCER=10% and 5%. In general, among the different data augmentation techniques, the multi-crop approach provides better results. Looking at the performance of the different networks, here we observe an opposite behavior with respect to the experiments on digital images: in fact, the best performing nets are the VGG-Face models pre-trained on large face datasets with AlexNet and VGG19 struggling to reach decent performance. Since P&S removes most of the digital artifacts we argue that more powerful and problem specific feature detectors are needed to solve such a complex problem.

To better analyze the effects of extending the digital training set with simulated P&S images the genuine and morphed score distributions of AlexNet and VGG-Face16 networks trained with the $Digital_{Au}$ and the $Digital_{Au} + P\&S_{Au}$ training sets are reported in Figure 15. The graphs clearly show that the networks trained on digital images only ($Digital_{Au}$) return a score close to 0 for both genuine and morphed images. This means that the modifications introduced by P&S remove the textural details that makes genuine and morphed images distinguishable. When training is extended with simulated P&S images ($Digital_{Au} + P\&S_{Au}$), the network pre-trained on face images (VGG-Face16) is able to learn P&S specific features making it able to discriminate genuine from morphed images. Therefore, the genuine scores become higher, while the morphed scores are generally kept quite low, as clearly visible by the score distributions for VGG-Face16. On the contrary AlexNet does not benefit of this further training step whose introduction determines an increment of all the scores (genuine and morphed).

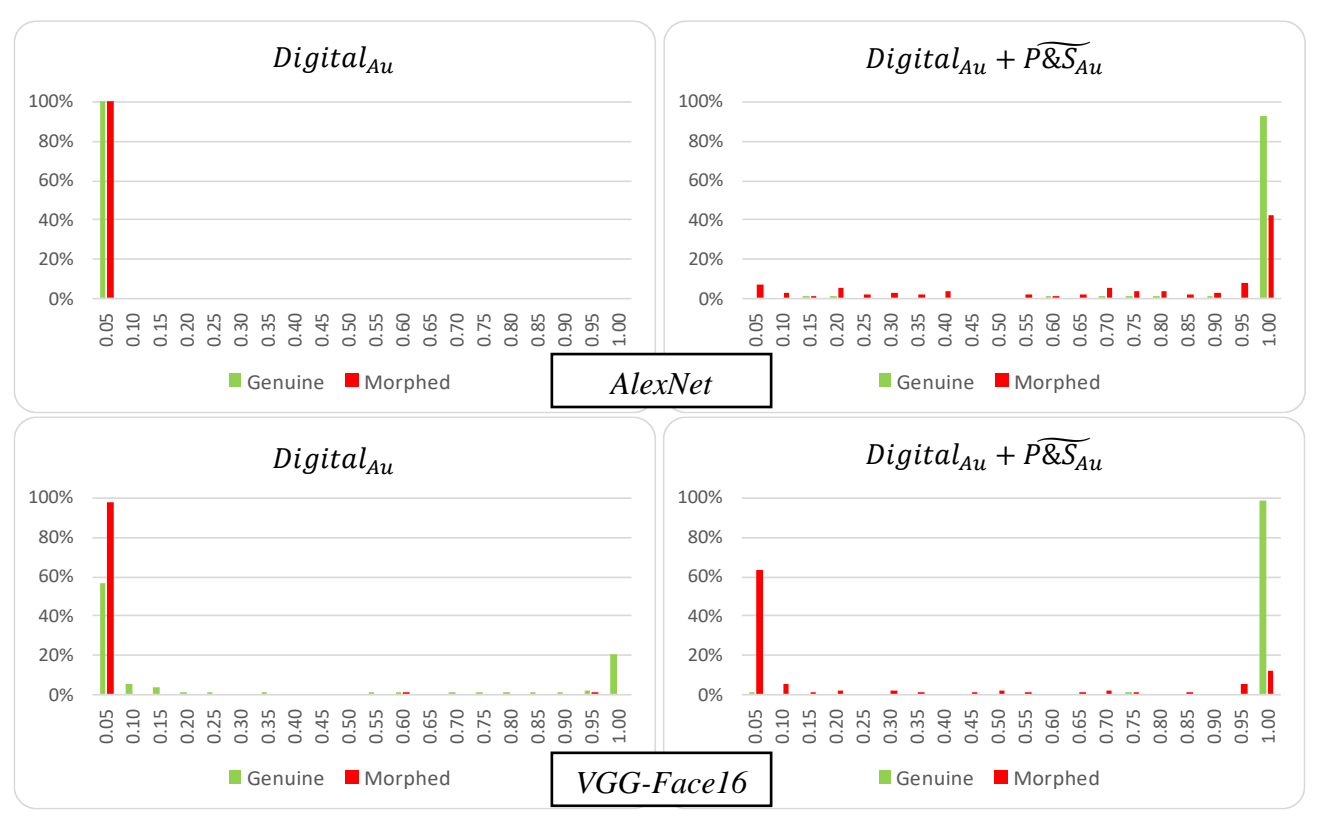


Figure 15: Genuine and morphed score distribution on $MorphDB_{P\&S}$ for AlexNet and VGG-Face16 networks obtained using the $Digital_{Au}$ training set (1st column) and the $Digital_{Au} + P\&S_{Au}$ training set (2nd column).

6.3. Evaluating networks as feature extractors

The results obtained using networks as feature extractors on digital and P&S images are provided in Table 5 and Table 6, respectively. In both experiments the networks used for feature extraction are tuned using augmented training sets (e.g., $Digital_{Au}$) while the external classifiers are trained on features extracted from datasets without any augmentation (e.g., Digital); this training strategy is referred to as $Digital_{Au}/Digital$ in the following.

Figure 16 shows the DET curves obtained for the different networks coupled with SVM and P-CRC classifiers on $MorphDB_D$ and Biometix testing databases, while Figure 17 shows the DET curves on $MorphDB_{P\&S}$ using the $Digital_{Au}/Digital$ and the $Digital_{Au}+P\&S_{Au}/P\&S$ training sets.

As to the digital databases, the results obtained are very good, with a slightly better behavior of the SVM classifier with respect to P-CRC. Also in this case, the different approaches perform better on $MorphDB_D$ than on Biometix database.

As to the tests on $MorphDB_{P\&S}$ using only digital images for training, the experiments confirm the incapacity of discriminating genuine and morphed images observed for the tested networks (see Table 4). When a fine-tuning on simulated P&S images is performed, the performance improvement is confirmed for networks pre-trained on face images (VGG-Face16 and VGG-Face2).

In conclusion, the evaluated networks seem to provide better results when directly used for image classification (fine-tuning), even if also when used for feature extraction provide very good results on the digital images.

Table 5: Performance indicators on the $MorphDB_D$ and Biometix testing databases using $Digital_{Au}/Digital$ as training set. The best result on each test database is highlighted in bold.

Test	Features	Classifier	Accuracy	EER	E	BPCER (%) at	
Test	1 catales	Classifici	(%)	(%)	APCER 10%	APCER 5%	APCER 1%
	AlexNet – fc6	Linear SVM	97.8	2.2	0.8	0.8	10.8
		P-CRC	97.4	3.9	2.3	3.8	16.9
	VGG19 – fc6	Linear SVM	95.7	4.8	0.8	3.8	11.5
$MorphDB_D$		P-CRC	94.3	4.8	0.0	3.1	26.9
I I	VGG-Face16 – fc6	Linear SVM	95.7	3.4	1.5	1.5	22.3
	V G G T ucc 10 100	P-CRC	94.8	3.4	1.5	3.1	16.2
	VGG-Face2 -	Linear SVM	95.2	1.3	0.0	0.0	1.5
	pool5/7x7_s1	P-CRC	94.3	0.4	0.0	0.0	0.8
	AlexNet – fc6	Linear SVM	97.9	2.3	0.2	1.0	3.8
		P-CRC	98.1	8.5	7.0	13.6	47.6
	VGG19 – fc6	Linear SVM	98.9	1.2	0.0	0.0	1.2
Biometix		P-CRC	98.4	3.0	0.0	0.9	27.9
	VGG-Face16 – fc6	Linear SVM	87.9	11.5	14.5	28.2	60.0
		P-CRC	87.0	17.6	36.1	60.4	83.0
	VGG-Face2 -	Linear SVM	89.4	10.6	11.0	22.6	53.4
	pool5/7x7_s1	P-CRC	89.2	11.2	13.1	21.5	46.8

Table 6: Performance indicators on the $MorphDB_{P\&S}$ testing database using different training sets. The best results are highlighted in bold.

Features	Training (Feature	Classifier	Accuracy	EER BPCER (%) at			
1 carares	Extractor/Classifier)	Classifici	(%)	(%)	APCER=10%	APCER=5%	APCER=1%
	Digital _{Au} /Digital	Linear SVM	43.5	26.5	50.8	57.7	64.6
AlexNet – fc6	= 191111Au/ = 1911111	P-CRC	43.5	26.5	51.5	64.6	78.5
	$Digital_{Au} + P\widetilde{\&S_{Au}}/\widetilde{P\&S}$	Linear SVM	60.9	20.0	45.5	60.0	71.5
	- 19 1111 Au - 1 112 Au / 1 112	P-CRC	63.9	46.1	87.7	89.2	95.4
	Digital _{Au} /Digital	Linear SVM	44.8	29.1	53.8	69.2	85.4
VGG19 – fc6	= 191111AU1 = 1911111	P-CRC	45.2	34.8	65.4	72.3	86.9
	$Digital_{Au} + P \widetilde{\&S}_{Au} / P \widetilde{\&S}$	Linear SVM	62.6	19.1	40.0	42.3	52.3
		P-CRC	62.2	45.7	92.3	95.4	98.5
	Digital _{Au} /Digital	Linear SVM	57.4	10.0	10.0	36.2	74.6
VGG-Face16 –		P-CRC	60.0	17.0	23.1	33.8	71.5
fc6	$Digital_{Au} + \widetilde{P\&S_{Au}}/\widetilde{P\&S}$	Linear SVM	90.4	6.1	4.6	7.7	53.1
		P-CRC	89.1	7.8	5.4	10.0	47.7
	Digital _{Au} /Digital	Linear SVM	52.6	19.6	23.1	29.2	53.1
VGG-Face2 -	3Au1 = 13	P-CRC	52.6	22.2	41.5	46.9	56.9
pool5/7x7_s1	$Digital_{Au} + P \widetilde{\&S}_{Au} / P \widetilde{\&S}$	Linear SVM	80.0	9.6	8.5	14.6	33.8
	$Bigitut_{Au} + I & S_{Au}/I & S$	P-CRC	75.2	9.6	6.2	20.8	70.0

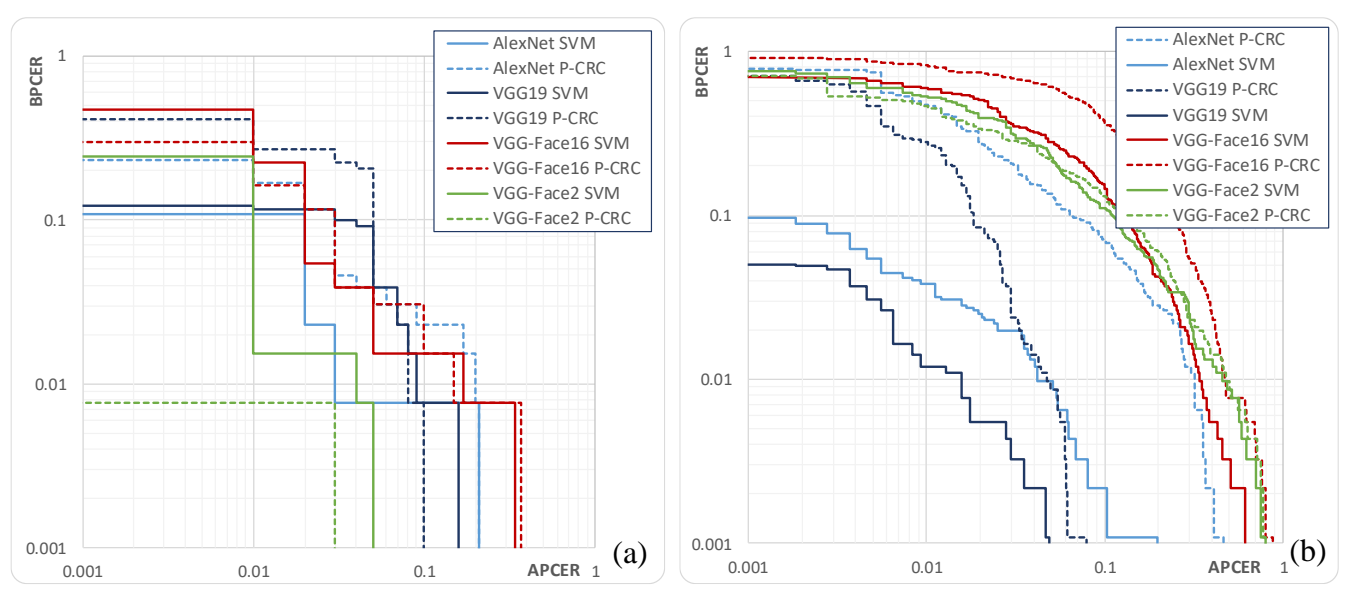


Figure 16: DET curves measured for the different networks combined with SVM and P-CRC classifiers trained using digital images (Digital) and tested on $MorphDB_D$ (a) and Biometix (b) databases.

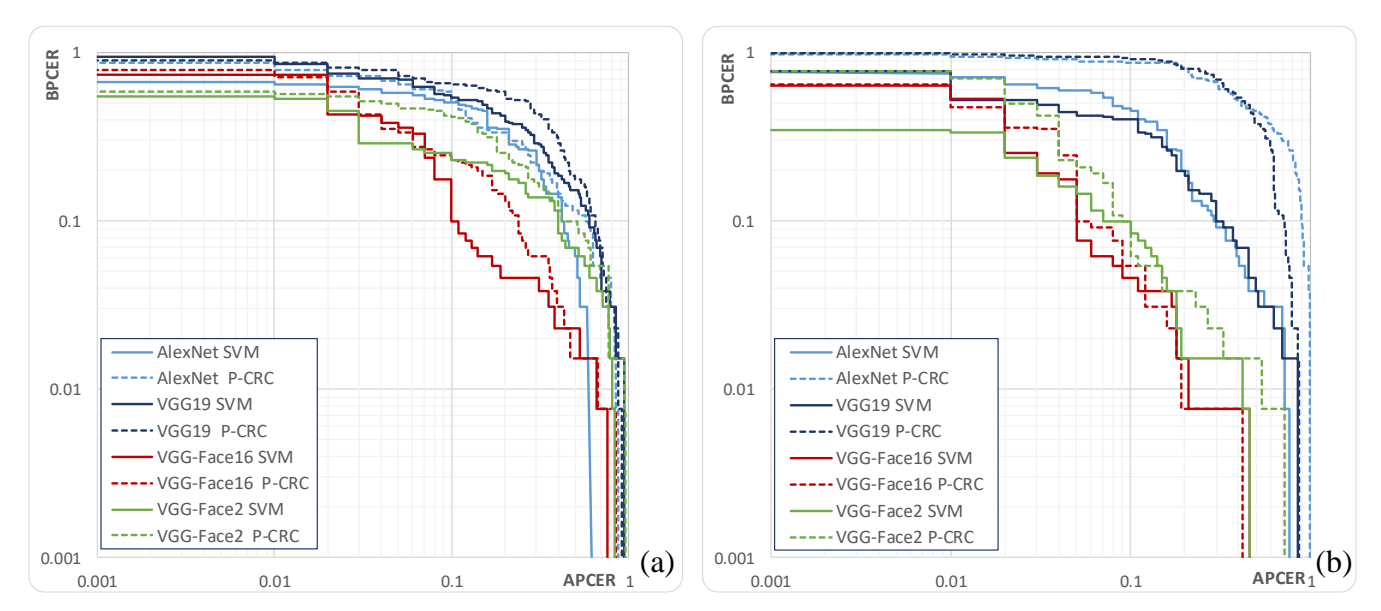


Figure 17: DET curves measured for the different networks combined with SVM and P-CRC classifiers on $MorphDB_{P\&S}$: (a) results with the Digital training set, (b) results with the $Digital + \widetilde{P\&S}$ training set.

7. Conclusions

In this work, different network architectures have been used for single image face morphing detection in both digital and P&S scenarios. In particular, we focused on P&S images, which today still represents a big challenge as confirmed by the results reported in Table 7 where the performance of recently proposed algorithms for digital and P&S images are summarized. Please note that a direct comparison is not possible because different datasets and protocols have been used but overall the results clearly show the difficulty of dealing with P&S. Our initial experiments proved that good performance can be achieved on digital images (BPCER=0% at APCER=10%), confirming the effectiveness of different networks already discussed in [17] [22] [23]. Unfortunately such low error rates cannot be extended to P&S images (BPCER about 12% at APCER=10%) if only digital images are used for training. To overcome this problem, an automatic generation procedure has been proposed to simulate the typical P&S image degradation. When combined with automatic morphing generation it allows to produce a

vast amount of training data for network training/tuning without the costs/efforts needed to manually print and scan face images.

The use of simulated P&S images allowed to significantly improve morphing detection performance, achieving a BPCER=2.3% at APCER=10% which is, to the best of our knowledge, a state-of-the-art result for P&S images (see Table 7). The obtained results are quite promising also considering that the demorphing approach proposed in [26], exploiting a second image as helper, when tested on the same dataset ($MorphDB_{P\&S}$) shows comparable performance (BPCER about 0.8% at APCER 10%).

Table 7: Summary of results for recently proposed morphing detection approaches (single image) on various digital and P&S datasets. Note that a direct comparison is not feasible since different databases and protocols have been used.

Image	Approach	Accuracy	EER	R BPCER (%) at		
type	pp-owe	(%)	(%)	APCER 10%	APCER 5%	APCER 1%
	[13]	98.4	-	-	-	-
	[22]	-	8.2	7.5	14.4	-
	[23]	-	-	-	-	~3.5
	[24]	-	3.1	-	-	-
	[29]	-	3.3	-	-	-
	[20]	-	32.7	61.7	-	-
Digital	[25]	-	2.8	0.7	1.8	-
	[5]	-	7.1	5.6	11.7	-
	[16]	-	2.5	-	-	-
	[17]	93.6	-	-	-	-
	[18]	-	-	-	-	~1.0
	[19]	-	2.2	0.1	0.6	-
	Proposed approach	99.3	0.9	0.0	0.0	0.9
	[22]	-	12.5	16.4	28.8	-
P&S	[5]	-	20.7	22.4	44.2	-
	[21]	82.4	-	-	-	-
	Proposed approach	93.5	6.1	2.3	6.9	43.8

Since the size of our training databases does not allow to train large models from scratch, all the CNN used in this work were pre-trained. The experiments highlighted that CNN pre-trained on natural images (ImageNet) can perform well on digital images, while CNN specifically pre-trained on face images (VGG Face datasets) perform better on P&S images. We argue that to detect textural differences between genuine and morphed (digital) images, the filters learned from natural images are quite good, while in presence of P&S images more sophisticated and face-specific filters are necessary to detect the fine artifacts that survive the printing and scanning process. Some preliminary works [24], aimed at understanding the factors influencing the network decision, analyzed the importance of different face regions for morphing detection on digital images. Further studies are necessary to better understand and explain these phenomena especially on P&S images: we believe that existing visualization techniques (see [49]) can be profitably used to this purpose.

Recently Generative Adversarial Networks (GAN) [50] have been successfully used for various image generation applications (e.g., [51]); their adoption for P&S simulation will be studied in our future researches.

Finally, since performance are datasets dependent, and the specific morphing technique used has a noticeable impact on the morphing detection accuracy, we believe that the availability of common

datasets and/or benchmarks is fundamental for the research community. To this purpose, a valuable contribution comes from NIST with the Face Recognition Vendor Test (FRVT) MORPH competition [52], to which we plan to submit our algorithm in the near future.

References

- [1] M. Ferrara, A. Franco, and D. Maltoni, "On the Effects of Image Alterations on Face Recognition Accuracy," in *Face Recognition Across the Electromagnetic Spectrum*. Switzerland: Springer International Publishing, 2016, pp. 195-222.
- [2] M. Ferrara, A. Franco, and D. Maltoni, "The Magic Passport," in *IEEE International Joint Conference on Biometrics (IJCB)*, Clearwater, Florida, USA, 2014, pp. 1-7.
- [3] M. Gomez-Barrero, C. Rathgeb, U. Scherhag, and C. Busch, "Is your biometric system robust to morphing attacks?," in *5th International Workshop on Biometrics and Forensics (IWBF)*, Coventry, UK, 2017.
- [4] M. Gomez-Barrero, C. Rathgeb, U. Scherhag, and C. Busch, "Predicting the vulnerability of biometric systems to attacks based on morphed biometric information," *IET Biometrics*, vol. 7, no. 4, pp. 333-341, June 2018.
- [5] U. Scherhag et al., "On the vulnerability of face recognition systems towards morphed face attacks," in 5th International Workshop on Biometrics and Forensics (IWBF), Coventry, UK, 2017.
- [6] (2019, January) Labeled Faces in the Wild. [Online]. http://vis-www.cs.umass.edu/lfw/
- [7] A. Krizhevsky, I. Sutskever, and G. E. Hinton, "ImageNet classification with deep convolutional neural networks," in *25th International Conference on Neural Information Processing Systems* (NIPS), Lake Tahoe, Nevada, 2012, pp. 1097-1105.
- [8] K. Simonyan and A. Zisserman, "Very Deep Convolutional Networks for Large-Scale Image Recognition," arXiv, 2015.
- [9] A. Makrushin and A. Wolf, "An Overview of Recent Advances in Assessing and Mitigating the Face Morphing Attack," in *26th European Signal Processing Conference (EUSIPCO)*, Rome, Italy, 2018.
- [10] R. Raghavendra, K. B. Raja, and C. Busch, "Detecting morphed face images," in *IEEE 8th International Conference on Biometrics Theory, Applications and Systems (BTAS)*, Niagara Falls, NY, 2016.
- [11] T. Neubert, "Face Morphing Detection: An Approach Based on Image Degradation Analysis," in *International Workshop on Digital Watermarking (IWDW)*, Magdeburg, Germany, 2017, pp. 93-106.
- [12] A. Makrushin, C. Kraetzer, T. Neubert, and J. Dittmann, "Generalized Benford's Law for Blind Detection of Morphed Face Images," in *6th ACM Workshop on Information Hiding and Multimedia Security*, Innsbruck, Austria, 2018, pp. 49-54.

- [13] A. Makrushin, T. Neubert, and J. Dittmann, "Automatic Generation and Detection of Visually Faultless Facial Morphs," in *12th International Joint Conference on Computer Vision, Imaging and Computer Graphics Theory and Applications*, Porto, Portugal, 2017.
- [14] M. Hildebrandt, T. Neubert, A. Makrushin, and J. Dittmann, "Benchmarking face morphing forgery detection: Application of stirtrace for impact simulation of different processing steps," in 5th International Workshop on Biometrics and Forensics (IWBF), Coventry, UK, 2017.
- [15] C. Kraetzer, A. Makrushin, T. Neubert, M. Hildebrandt, and J. Dittmann, "Modeling Attacks on Photo-ID Documents and Applying Media Forensics for the Detection of Facial Morphing," in 5th ACM Workshop on Information Hiding and Multimedia Security, Philadelphia, Pennsylvania, USA, 2017, pp. 21-32.
- [16] L. Spreeuwers, M. Schils, and R. Veldhuis, "Towards Robust Evaluation of Face Morphing Detection," in *26th European Signal Processing Conference (EUSIPCO)*, Rome, Italy, 2018.
- [17] L. Wandzik, G. Kaeding, and R. V. Garcia, "Morphing Detection Using a General- Purpose Face Recognition System," in *26th European Signal Processing Conference (EUSIPCO)*, Rome, Italy, 2018.
- [18] L. B. Zhang, F. Peng, and M. Long, "Face Morphing Detection Using Fourier Spectrum of Sensor Pattern Noise," in *IEEE International Conference on Multimedia and Expo (ICME)*, San Diego, CA, USA, 2018.
- [19] L. Debiasi, U. Scherhag, C. Rathgeb, A. Uhl, and C. Busch, "PRNU-based detection of morphed face images," in *International Workshop on Biometrics and Forensics (IWBF)*, Sassari, Italy, 2018.
- [20] U. Scherhag, D. Budhrani, M. Gomez-Barrero, and C. Busch, "Detecting Morphed Face Images Using Facial Landmarks," in *International Conference on Image and Signal Processing (ICISP)*, Cherbourg, France, 2018, pp. 444-452.
- [21] S. Jassim and A. Asaad, "Automatic Detection of Image Morphing by Topology-based Analysis," in *26th European Signal Processing Conference (EUSIPCO)*, Rome, Italy, 2018.
- [22] R. Raghavendra, K. B. Raja, S. Venkatesh, and C. Busch, "Transferable Deep-CNN Features for Detecting Digital and Print-Scanned Morphed Face Images," in *IEEE Conference on Computer Vision and Pattern Recognition Workshops (CVPRW)*, Honolulu, HI, USA, 2017.
- [23] C. Seibold, W. Samek, A. Hilsmann, and P. Eisert, "Detection of Face Morphing Attacks by Deep Learning," in *International Workshop on Digital Watermarking (IWDW)*, Magdeburg, Germany, 2017, pp. 107-120.
- [24] C. Seibold, W. Samek, A. Hilsmann, and P. Eisert, "Accurate and Robust Neural Networks for Security Related Applications Exampled by Face Morphing Attacks," arXiv, 2018.
- [25] U. Scherhag, C. Rathgeb, and C. Busch, "Morph Deterction from Single Face Image: a Multi-Algorithm Fusion Approach," in *2nd International Conference on Biometric Engineering and Applications (ICBEA)*, Amsterdam, Netherlands, 2018, pp. 6-12.
- [26] M. Ferrara, A. Franco, and D. Maltoni, "Face Demorphing," *IEEE Transactions on Information Forensics and Security*, vol. 13, no. 4, pp. 1008-1017, April 2018.

- [27] M. Ferrara, A. Franco, and D. Maltoni, "Face Demorphing in the Presence of Facial Appearance Variations," in *European Signal Processing Conference (EUSIPCO)*, Rome, Italy, 2018.
- [28] U. Scherhag, C. Rathgeb, and C. Busch, "Towards detection of morphed face images in electronic travel documents," in *13th IAPR International Workshop on Document Analysis Systems (DAS)*, Vienna, Austria, 2018.
- [29] U. Scherhag, C. Rathgeb, and C. Busch, "Performance variation of morphed face image detection algorithms across different datasets," in *International Workshop on Biometrics and Forensics* (*IWBF*), Sassari, Italy, 2018.
- [30] C. Lin and S. Chang, "Distortion Modeling and Invariant Extraction for Digital Image Print-and-Scan Process," in *International Symposium on Multimedia Information Processing (ISMIP)*, Taipei, Taiwan, 1999.
- [31] L. Taylor and G. Nitschke, "Improving Deep Learning using Generic Data Augmentation," arXiv, 2017.
- [32] Xiberpix. (2019, January) Sqirlz Morph 2.1 Web Site. [Online]. http://www.xiberpix.net/SqirlzMorph.html
- [33] S. A. Robila, "Using spectral distances for speedup in hyperspectral image processing," *International Journal of Remote Sensing*, vol. 26, no. 24, pp. 5629-5650, December 2005.
- [34] A. M. Martinez and R. Benavente, "The AR face database," Computer Vision Center, CVC Technical Report 1998.
- [35] P. J. Phillips et al., "Overview of the face recognition grand challenge," in *proceedings IEEE Computer Vision and Pattern Recognition*, vol. 1, 2005, pp. 947-954.
- [36] P. J. Phillips, H. Wechsler, J. Huang, and P. J. Rauss, "The FERET database and evaluation procedure for face-recognition algorithms," *Image and Vision Computing*, vol. 16, no. 5, pp. 295–306, April 1998.
- [37] P. J. Phillips, H. Moon, S. A. Rizvi, and P. J. Rauss, "The FERET evaluation methodology for face-recognition algorithms," *IEEE Transactions on Pattern Analysis and Machine Intelligence*, vol. 22, no. 10, pp. 1090-1104, October 2000.
- [38] Biometix Pty Ltd 2018. (2019, January) New Face Morphing Dataset (for vulnerability research). [Online]. http://www.biometix.com/2017/09/18/new-face-morphing-dataset-for-vulnerability-research/
- [39] Neurotechnology Inc. (2019, January) Neurotechnology Web Site. [Online]. http://www.neurotechnology.com/
- [40] J. Deng et al., "ImageNet: A large-scale hierarchical image database," in *IEEE Conference on Computer Vision and Pattern Recognition*, Miami, FL, USA, 2009, pp. 248-255.
- [41] (2019, January) BVLC AlexNet Caffe Model. [Online]. https://github.com/BVLC/caffe/tree/master/models/bvlc_alexnet

- [42] O. Russakovsky et al., "ImageNet Large Scale Visual Recognition Challenge," *International Journal of Computer Vision*, vol. 115, no. 3, pp. 211-252, December 2015.
- [43] O. M. Parkhi, A. Vedaldi, and A. Zisserman, "Deep Face Recognition," in *British Machine Vision Conference (BMVC)*, 2015, pp. 41.1-41.12.
- [44] Q. Cao, L. Shen, W. Xie, O. M. Parkhi, and A. Zisserman, "VGGFace2: A Dataset for Recognising Faces across Pose and Age," in 13th IEEE International Conference on Automatic Face & Gesture Recognition (FG 2018), Xi'an, China, 2018.
- [45] K. He, X. Zhang, S. Ren, and J. Sun, "Deep Residual Learning for Image Recognition," in *IEEE Conference on Computer Vision and Pattern Recognition (CVPR)*, Las Vegas, NV, USA, 2016, pp. 770-778.
- [46] V. N. Vapnik, Statistical Learning Theory.: John Wiley & Sons, 1998.
- [47] S. Cai, L. Zhang, W. Zuo, and X. Feng, "A Probabilistic Collaborative Representation Based Approach for Pattern Classification," in *IEEE Conference on Computer Vision and Pattern Recognition (CVPR)*, Las Vegas, NV, USA, 2016.
- [48] International Organization for Standardization (ISO), "Information Technology Biometric presentation attack detection Part 3: Testing and reporting," Geneva, Switzerland, ISO/IEC FDIS 30107-3:2017 JTC 1/SC 37, 2017.
- [49] C. Olah, A. Mordvintsev, and L. Schubert, "Feature Visualization," *Distill*, 2017.
- [50] I. Goodfellow et al., "Generative Adversarial Nets," in *Conference on Neural Information Processing Systems (NIPS)*, Montreal, Quebec, Canada, 2014.
- [51] F. Peng, L. B. Zhang, and M. Long, "FD-GAN: Face-demorphing generative adversarial network for restoring accomplice's facial image," arXiv, 2018.
- [52] NIST. (2019, January) Face Recognition Vendor Test (FRVT) MORPH. [Online]. https://www.nist.gov/programs-projects/face-recognition-vendor-test-frvt-morph